The 2010 IEEE/RSJ International Conference on
Intelligent Robots and Systems
October 18-22, 2010, Taipei, Taiwan

Biomimetic Sonar: 3D-Localization of Multiple Reflectors

Filips Schillebeeckx and Herbert Peremans

Abstract— **This paper presents an advanced bio-inspired binaural sonar sensor capable of localizing multiple reflectors in 3D-space with a single measurement. The system makes use of spectral cues in the received echoes only. Two artificial pinnae act as complex direction-dependent spectral filters on the echoes returning from the insonified reflectors. A maximum likelihood estimator is used to select the best azimuth-elevation pair based on the calculated a posteriori probability for all target angles, given the measured target spectrum. Experimental results in which three targets are localized simultaneously are presented.**

I. Introduction

Irrespective of the specific task, mobile robot performance is directly linked to the amount and quality of information the robot receives about its direct environment from its various sensor systems. Therefore, there is an ongoing effort to improve each of the commonly used sensor modalities such as vision, laser-ranging or sonar-ranging. Each of these modalities has advantages and drawbacks, be it cost, size, reliability, refresh rate, computational cost, susceptibility to changing light conditions, presence of smoke, reflective surfaces, etc... In non-structured environments, it seems reasonable that a multi-modal approach greatly enhances a system's overall robustness to varying environment conditions and its ability to overcome the problem of perceptual aliasing.

While a lot of effort has been given to the improvement of laser-ranging and vision systems, in-air sonar is predominantly used for obstacle avoidance only. However, advanced sonar sensor systems for robots are a low cost and complementary sensor modality to optical systems [1]. Also, bats have adequately shown that in-air sonar can provide sufficient navigational cues in complex environments [2], [3].

Advanced sonar sensors have been developed for robust mapping and indoor localization in indoor environments [4] and systems capable of single cycle classification of planes, corners and edges have been reported [5], [6]. Some sensor developers have focused on the subtask of target localization using triangulation methods based on ITD-cues, i.e. interaural time difference [7], [8], [9], [10], [11]. However, the independent noise-component affecting time-of-flight determination gets amplified with decreasing interaural distance.

The system presented here mimics the bat's echolocation system in an attempt to extract as much spatial information as possible with a minimal number of components, i.e. only one emitter and two receivers. Contrary to most other sonar systems, it does not make use of ITD-cues, but instead extracts scene information from a single broadband measurement based on spectral cues only. This study shows that it is possible to localize multiple objects in 3D-space with a binaural bio-inspired sonar head, using fairly simple technology and a straightforward probabilistic method.

Experiments have shown that echolocating bats use information extracted from the systematic variations in the spectrum of the received echo as a function of the reflecting target position, as localization cues [12]. Previous work has described how a binaural system based on Polaroid transducers can extract target range and azimuth, i.e. 2D-position, from spectral information only [13]. Building a sensor system with a more complex directivity, thereby improving the system's ability to localize reflectors both in azimuth and elevation, extends this approach to full 3D-localization. Although the use of spectral cues for target localization with active sonar systems has been investigated to some degree ([14], [15]), none of these systems have demonstrated 3D-localization of real reflectors with a single, binaural, active sonar measurement in realistic noise conditions.

II. Biomimetic Sonar System

A. The Robotic Bat Head

Building a small sonar device requires receivers that are much smaller than the widely-used Polaroid transducers, but such receivers (e.g. the Knowles FG-23329 used in this research) are virtually omni-directional [16] and therefore lack the required spatial directivity characteristics. In order to enhance their fitness for localization tasks, it is necessary to artificially improve the spatial directivity characteristics of the receivers. Interestingly, the complex spatial filtering of various bat pinnae has been extensively described to do just that [2]. Inspired by its biological counterpart, we have mimicked this approach in the sonar device presented here.

All experiments were performed with the Circe head (fig. 1), equipped with two artificial *Phyllostomus discolor* pinnae [17]. The head was mounted on a 'neck' platform which can be panned between -45° and +45° and tilted between -36° and +36° (full range). In each of the two artificial pinnae, a Knowles FG-23329 microphone was inserted at the end of the ear canal. Fig. 2 shows a schematic of the measurement setup and the angle conventions used throughout the paper.

B. Spectral Code Extraction

After each emission, the two receivers pick up echoes from reflectors that are located within the insonified area.

This work was supported by the EU, IST-FET Program, as part of the CILIA [grant number FP6-016039] project and the University of Antwerp BOF-UA Program supporting interdisciplinary Ph.D-research.

F. Schillebeeckx is with Departement of Math. and Comp. Science, Univ. of Antwerp, Belgium filips.schillebeeckx@ua.ac.be

H. Peremans is with the Dept. MTT , Fac. of TEW, Univ. of Antwerp, Belgium herbert.peremans@ua.ac.be

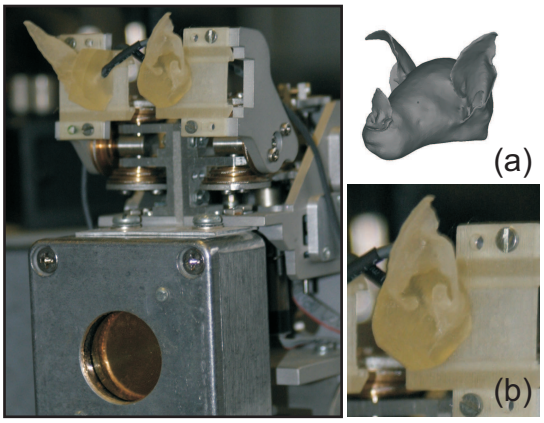

Fig. 1. Left: Circe sonar head with two artificial *Phyllostomus discolor* pinnae and emitter. (a) Virtual 3D-model of a scanned *Phyllostomus discolor* head. (b) Close-up of the corresponding artificial pinna, which was cut from the virtual model, merged with a support structure model and finally 3D-printed

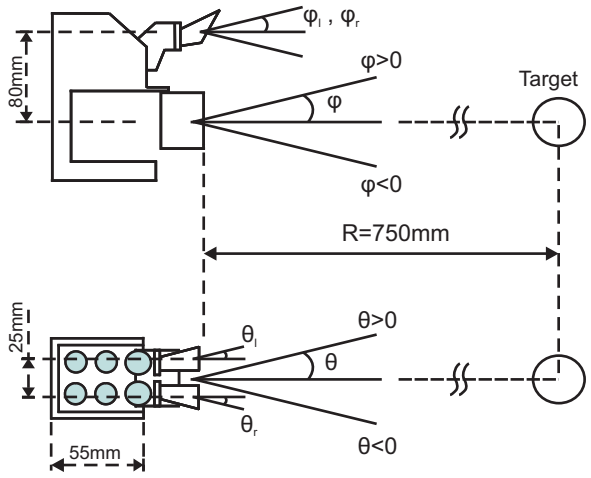

Fig. 2. Schematic drawing of the measurement setup. θ (azimuth) and ϕ (elevation) represent target angles. Top: targets above the horizontal plane ϕ=0 have positive ϕ-values. Bottom: targets on the side of the left ear with respect to the vertical plane θ=0 have positive θ-values. The non-zero dimensions of the sonar head are known, therefore θ_l,θ_r, and ϕ_l,ϕ_r can be calculated from θ, ϕ and the distance to the reflector R.

Each of these echoes is a filtered version of the fm-call and can be represented in the frequency-domain by a spectral code. The process of extracting such a spectral code is described at length in [13] and visualized in fig. 3 for a single wave form. In the current paper, an 70-channel gammatone filterbank with center frequencies from 100kHz-30kHz and Q-factor 50 is used to construct a spectrogram of the two echo signals. By time shifting all frequency channels with a value corresponding to the frequency-dependent time delays in the emitted fm-call, a dechirped representation is constructed. An echo spectral code can then be extracted for each reflector by selecting the values corresponding to the local maximum in the summed energy of the dechirped spectrograms, as illustrated in fig. 3(c). The binaural spectral code is constructed by concatenating the two individual spectral codes for a given reflector. Because of the dechirping process, pulse overlap is not determined by chirp pulse length, but by the duration of the responses of the filters in the chosen filter bank. The term 'spectral code' is used because the extraction method does not return the exact echo spectrum, i.e. the Fourier transform of the returning wave form, but a close approximation instead. Note that this scheme makes use of the prior knowledge of the time-frequency representation of the emitted call (cf. matched filter). Also, the distances r_i to different targets are easily extracted from the dechirped spectrogram representation.

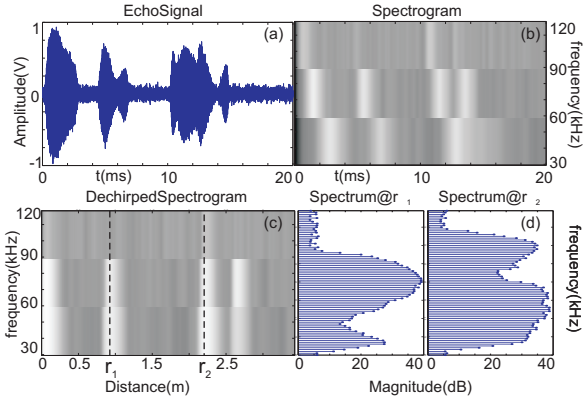

Fig. 3. Visualization of the (monaural) spectral code extraction method: (a) Wave form representing the picked up call and three echoes, with the last two overlapping in time. (b) Spectrogram representation of the gammatone filterbank response. Each echo is a filtered version of the emitted fm-call (c) The dechirping process aligns the individual frequency channel responses. The spectra of partially overlapping echoes are separated in time/distance. (d) Two individual spectral codes, extracted at distances r_1 and r_2.

III. Direction-Dependent Spectral Filtering

Pinna filtering introduces systematic variations in the spectral code of a received echo, depending on the reflector location. This direction-dependent filtering is conventionally described by the head related transfer function (HRTF). However, to investigate active binaural echolocation, the complete sound path has to be taken into account, i.e. not only the HRTF of a single pinna, but also the transmitter radiation pattern, air filtering and reflector filtering.

The left and right receiver spectra S_l and S_r returning from a reflector at distance r, azimuth θ and elevation ϕ, in a noiseless environment, can be written as the result of a series of frequency-dependent spatial filter operations in the frequency domain:

$$S_l = H_l\left(\theta_l, \phi_l, f\right) \cdot H_a\left(r, f\right) \cdot H_{rfl}(\theta_l, \phi_l, f) \cdot X \quad (1)$$

$$S_r = H_r\left(\theta_r, \phi_r, f\right) \cdot H_a\left(r, f\right) \cdot H_{rfl}(\theta_r, \phi_r, f) \cdot X \quad (2)$$

with

$$X = H_a\left(r, f\right) \cdot H_{tr}\left(\theta, \phi, f\right) \cdot X_c\left(f\right) \quad (3)$$

where H_{tr}, H_a, H_{rfl}, H_l and H_r describe the filtering characteristics of transmitter, air, reflector, left and right receiver assembly respectively. (All frequency domain formulas in this paper describe magnitude effects only. Vertical

bars are therefore omitted to shorten notation.) X is the spectrum of the sound wave reaching the reflector.

To measure the direction-dependent filtering characteristics of the sonar system, we hung a wooden ball (70 mm diameter) at a distance of 0.75 m in front of the sonar head. Then, we moved its neck from positions θ_{neck}=$-45°$ to θ_{neck}=$+45°$ (azimuth) and from ϕ_{neck}=$-36°$ to ϕ_{neck}=$+36°$ (elevation) in steps of $1°$. From each of these positions, the robot head emitted a series of 100 frequency modulated calls sweeping downwards from 120kHz-30kHz with a duration of 3ms. In each position, the resulting binaural mean echo spectral code was extracted and stored, forming a template set $T(\theta, \phi, f)$ containing the expected spectral code for each corresponding target angle (θ, ϕ).

Although the direction-dependent characteristics of the extracted monaural spectral codes are dominated by the circular-symmetric radiation pattern of the transmitter, they are also affected by the spatial selectivity of the pinna-receiver-assemblies. As a result, the binaural spectral codes returning from a reflector at different positions vary a great deal across the observed range and across frequencies. Results are shown in fig. 4 (left ear). The right ear results are similar (mirrored around the midsagittal plane).

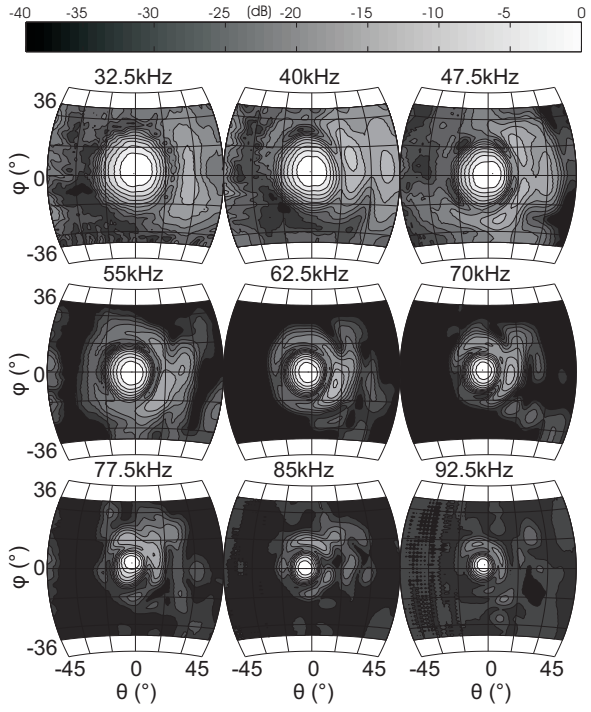

Fig. 4. Shaded contour plots of the direction-dependent characteristics of the measured spectral codes (left pinna only) for the ball reflector (frequencies 32.5-92.5kHz in 7.5kHz-intervals). Each plot represents a spherical projection of the frontal hemifield ($\pm 45°$ in azimuth, $\pm 36°$ in elevation, interval size $1°$). Isocontour lines of the spectral code magnitude relative to the maximum magnitude at each frequency are shown in 3dB-decrements.

IV. Spectrum based binaural 3D-Localization

Spectrum based 3D-localization uses the information contained in the binaural broadband spectral codes and assumes that filtering by air H_a, filtering by the reflector H_{rfl}, and distance effects (within limits) do not dominate the shape of the resultant binaural spectral code. After emission, a spectral code is extracted from the echo signal returning from an unknown reflector location. Based on this binaural spectral code S_x, consisting of a 2x70=140 dimensional vector, the estimation method will search for the most probable target angle (θ, ϕ) from which the echo could have returned.

First, each stored spectral template $T(\theta_j, \phi_k, f)$ is normalized to the energy of S_x, resulting in the normalized template set $T_x(\theta, \phi, f)$. This normalization step is a first order approximation to compensate for unknown reflector strength and spherical spreading losses.

Next, every normalized template spectrum $T_x(\theta_j, \phi_k, f)$ is compared to the received spectral code of the unknown reflector. Based on empirical evidence, the unknown reflector environment filtering is modeled as additive Gaussian noise when expressing the spectrum on logarithmic scale.

$$20log(S_x(f)) = \mathcal{N}(20log(T_x(f)), \Sigma) \tag{4}$$

Σ was constructed by accumulating experimental data, i.e. spectral codes extracted from measurements on various reflectors.

Finally, the reflector angle is estimated by selecting the maximum a posteriori probability using Bayes' theorem

$$\widehat{\theta} = max_{\bar{\theta}}[\ P(\bar{\theta}|S_x)\ ] = max_{\bar{\theta}}[\ \frac{P(S_x|\bar{\theta})\ P(\bar{\theta})}{P(S_x)}\ ] \tag{5}$$

In the absence of specific prior information, $P(\bar{\theta})$ is assumed to be uniform, resulting in a maximum likelihood estimator.

Fig. 5 illustrates a best and worst case scenario of this procedure by showing the probability distribution for two selected single 3D-position estimates. For each estimate, the reflector spectral code S_x is compared to all available template spectra $T(\theta, \phi, f)$, resulting in a $P(\bar{\theta}|S_x)$-value for each $\bar{\theta}$. Then, the angle-pair corresponding to the maximum value of $P(\bar{\theta}|S_x)$ is selected. The success of the estimation process depends on the resemblance between the measurement and the correct template spectral code. A good resemblance will result in a distinct maximum near the correct position (θ_j, ϕ_k), as seen in fig. 5(a). Poorer resemblance, due to noise conditions and/or outspoken reflector filtering, results in a larger area of uncertainty around the correct (θ_j, ϕ_k)-orientation or the appearance of ambiguous regions, as seen in fig. 5(b).

V. Binaural 3D-Localization: Multiple Reflectors

The 3D-localization procedure was tested by simultaneously localizing 3 reflectors from 81 sonar head orientations (θ_{neck}=$-40°$ to θ_{neck}=$40°$, in steps of $1°$). For each of these orientations, two different spectrograms were extracted: a high-SNR spectrogram SG_M by averaging over the spectrograms calculated from 5000 consecutive echoes and a low-SNR spectrogram SG_S extracted from a single emission echo. The spectra obtained from the SG_M-spectrogram simulate the spectral codes that would be extracted with a

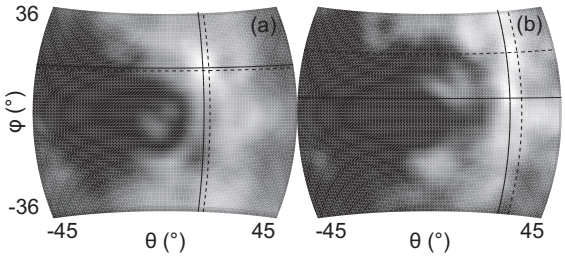

Fig. 5. Single estimation results depicting the probability distribution $P(\bar{\theta}|S_x)$ for all available $\bar{\theta}$, white being the highest values and darkening with decreasing probability. The correct position (θ_j, ϕ_k) is located on the intersection of the dashed lines. The estimated position $(\widehat{\theta}, \widehat{\phi})$ is located on the intersection of the full lines. (a) Target: θ_j=15°,ϕ_k=15°, estimated at $\widehat{\theta}$=13°,$\widehat{\phi}$=16° (b) Target: θ_j=31°,ϕ_k=21°, estimated at $\widehat{\theta}$=27°,$\widehat{\phi}$=5°

high-SNR acquisition system in noiseless conditions. The measurement setup is shown in fig. 6.

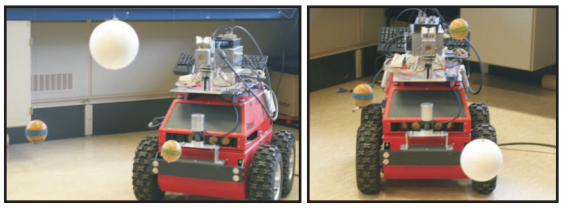

Fig. 6. Measurement Setup: 3 ball reflectors were hung in front of the sonar head in two separate experiments. Left: Experiment 1: Wooden ball T1 (r=0.75m, θ=6°, ϕ=−16°). Wooden ball T2 (r=1.0m, θ=−10°, ϕ=−8°). Styrofoam ball T3 (r=1.2m, θ=6°, ϕ=6°). Right: Experiment 2: Wooden ball T1 (r=0.76m, θ=6°, ϕ=13°). Wooden ball T2 (r=1.0m, θ=−10°, ϕ=3°). Styrofoam ball T3 (r=1.2m, θ=6°, ϕ=−5°).

A binaural spectral code was extracted from the spectrograms SG_S and SG_M at distances corresponding to each of the 3 targets. More specifically, each spectral code was extracted at the local energy maximum nearest to the expected target distance. For each of these three spectral codes, the angle-pair corresponding to the maximum probability $P(\bar{\theta}|S_x)$ is reported.

Fig. 7 shows the results of the first experiment. The range plots in fig. 7(a) demonstrate that all three targets are detected from all neck orientations, i.e. a local energy maximum is found for all three targets. The relative energy plots in fig. 7(b) indicate that the reflected energy is relatively peaked in a range of approximately 30° around the correct azimuth position, with the exception of target T1 for which the reflected energy is lower over the entire θ_{neck}-range because of its low elevation angle. This behavior is directly linked to the radiation pattern of the Polaroid transducer which emits most energy within a cone with aperture 30° at 50 kHz. An incorrect target (a wall cabinet) was detected at distance r=1.2m, explaining the rising edge in the energy plot for target T3 (head orientations $\theta_{neck} \leq -30°$). There is no significant difference in target detection performance between the results for SG_S and SG_M.

Fig. 7(c) and fig. 7(d) show the results for the azimuth and elevation estimation respectively. Overall, azimuth angles are well estimated within the entire θ_{neck}-range, indicating that the spectral code extracted from SG_M corresponds best to a template spectrum nearby the correct azimuth angle, even when reflected energy is (very) low. Sporadically the more noisy spectral codes extracted from SG_S lead to larger azimuth-errors, as can be expected. The elevation results are more error-prone. The elevation of targets T1 and T3 is estimated well throughout the θ_{neck}-range, but the elevation of target T2 is badly estimated in $\theta_{neck} = [-12°, -4°]$, even though the reflected energy is fairly high. In this range, an ambiguous template spectrum corresponding to an incorrect (θ, ϕ)-pair seems to be more similar to the extracted spectral code from SG_S and even SG_M than the one corresponding to the correct (θ, ϕ)-pair.

A second experiment was undertaken in which the elevations of the three targets were altered. Results are shown in fig. 8. Again, azimuths are well estimated for the entire range. Elevations are well estimated within the region of higher reflected energy. In a final experiment, target T1 of experiment 1 was moved to a larger azimuth ($\theta = 27°$). Results are shown in fig. 9. In this configuration the balls are wider apart, but can still be localized simultaneously in the range $\theta_{neck} = [-15°, 10°]$. Overall, the results are better for the spectra based on SG_M, but results for SG_S are not far behind. Also, azimuth is more robustly estimated than elevation, predominantly because the combined binaural spectrum also codes for IID-cues (interaural intensity differences). In effect, the binaural spectrum cues can be considered a superset of the IID-cues.

Table I contains summarizing numerical results for all three experiments. The first two columns list mean azimuth and elevation errors, the last two the ratio of estimates with an error of less than 3° to the total number of estimates, both within a given range. The best half-range is defined as the continuous subrange ($\Delta\theta_{neck} = 40°$) for which mean azimuth and elevation errors are minimal and the 3°-error estimate ratio is maximal, respectively. Note that the table features high 3°-error estimate ratios overall, including several scores of 1.00, i.e. for that particular range all azimuths and elevations were estimated with a 3°-error or less. The results of all three experiment clearly demonstrate that the 3D-localization method presented here can estimate reflector azimuth and elevation simultaneously based on binaural spectral information.

VI. Discussion and Conclusions

In this study, we have demonstrated that a binaural sonar sensor equipped with artificial bio-inspired pinnae can localize multiple reflectors in 3D-space. This shows that a spatial signature, largely determined by the transmitter radiation pattern, the pinna directivity and the interaction between them, can be successfully extracted from a binaural spectrogram representation of the echo.

A probabilistic model is used to derive the target angle probability distribution within the observable range based on the similarity between the measurement spectrum and template set spectra. Although the results presented are based on single estimations selecting the target angle with maximum

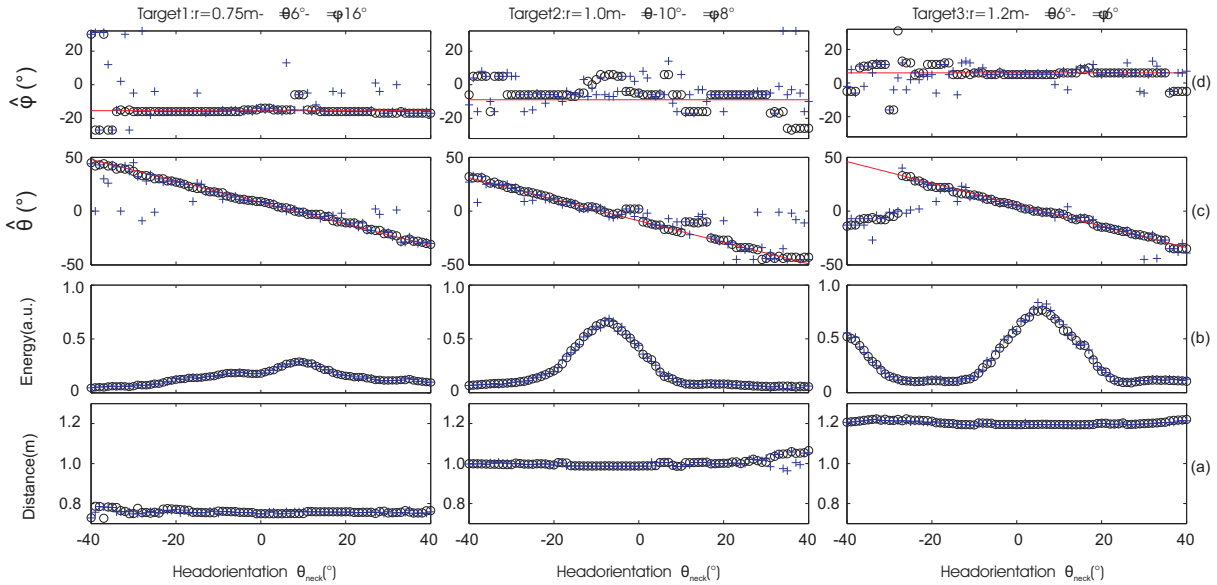

Fig. 7. Experiment 1: Wooden ball T1 (r=0.75m, θ=6°, ϕ=−16°). Wooden ball T2 (r=1.0m, θ=−10°, ϕ=−8°). Styrofoam ball T3 (r=1.2m, θ=6°, ϕ=6°). Each column displays the results of one of the three targets for each of the 81 orientations. In each plot, the results for SG_M are marked with a small circle, the results for SG_S with a plus-sign. Row (a): The distance at which the spectral code was extracted. Row (b): The relative energy corresponding to that spectral code. Row (c): The estimated azimuth $\widehat{\theta}$. A continuous line marks the correct azimuth angle θ. Row (d): The estimated elevation $\widehat{\phi}$. A continuous line marks the correct elevation angle ϕ.

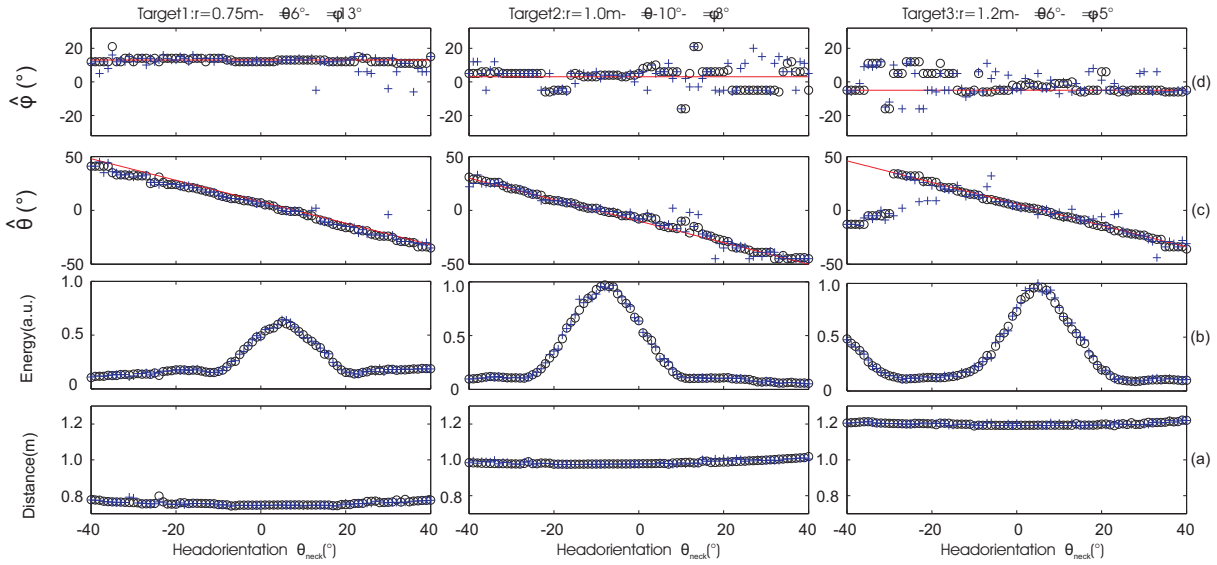

Fig. 8. Exp. 2: Wooden ball T1 (r=0.76m, θ=6°, ϕ=13°). Wooden ball T2 (r=1.0m, θ=−10°, ϕ=3°). Styrofoam ball T3 (r=1.2m, θ=6°, ϕ=−5°).

probability only, in effect resulting in a maximum likelihood estimator, the proposed method can be naturally extended to combine the information from consecutive measurements.

A number of improvements upon the current system can be envisaged. The localization method described here does not require pinna movement, therefore a miniaturized version of the larger Circe head could be constructed. Alternatively, ear mobility could be used for target position disambiguation by combining consecutive measurements with different pinna configurations. Furthermore, the binaural sonar system is an active sensor: the spectral content of the emitted call is known, and could be adapted for specific tasks.

Mobile robot navigation performance depends on the quality of the system's sensory inputs. Therefore, the search for sensors that provide a large information rate, i.e., accurate information within a large field of view at a high measurement rate, continues. We have demonstrated that it is possible to advance the potential of ultrasonic sensors by enhancing their directional properties by means of bio-inspired artificial pinnae. This enhanced directionality allows 3D-localization of real reflectors with a single, binaural active sonar measurement, in realistic noise conditions. In that sense, we believe the sonar system presented here is an example of how technical systems can benefit from knowledge and ideas

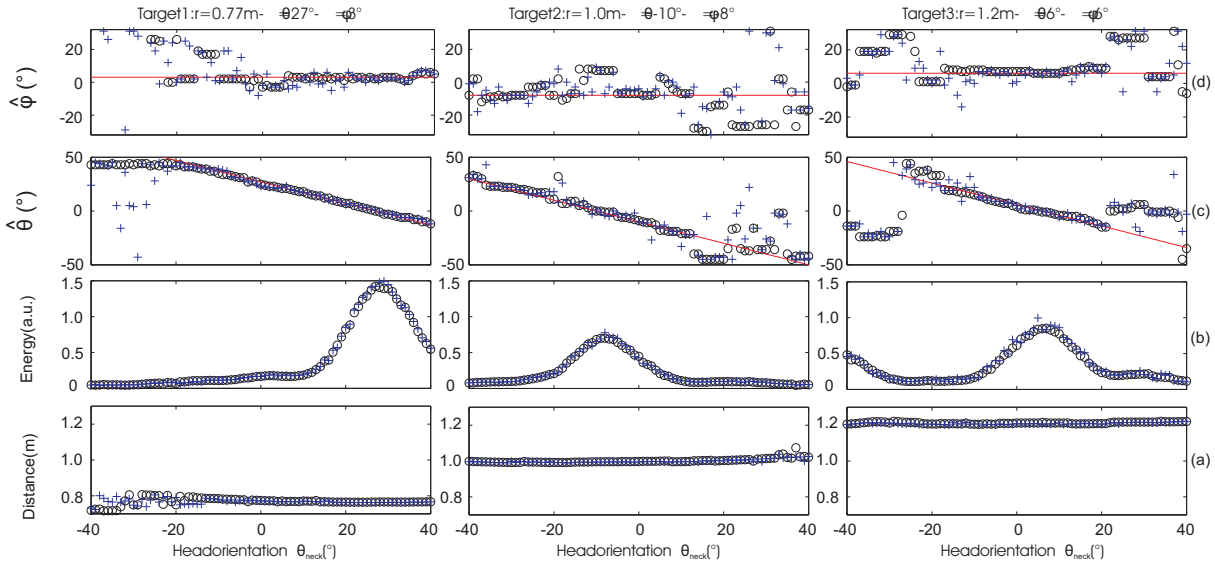

Fig. 9. Exp. 3: Wooden ball T1 (r=0.77m, θ=27°, ϕ=3°). Wooden ball T2 (r=1.0m, θ=−10°, ϕ=−8°). Styrofoam ball T3 (r=1.2m, θ=6°, ϕ=6°).

TABLE I

NUMERICAL RESULTS FOR ALL THREE EXPERIMENTS DISPLAYING THE BEST HALF-RANGE RESULTS ($\Delta\theta_{neck} = 40°$, N=41) AND THE FULL-RANGE RESULT (BETWEEN BRACKETS). THE FULL RANGE IS DEFINED AS $\Delta\theta_{neck} = 80°$, N=81 FOR T1 AND T2, $\theta_{neck} = [-20°, 40°]$ AND N=61 FOR T3.

T		$\frac{\sum\|\theta_i-\widehat{\theta_i}\|}{N}$	$\frac{\sum\|\phi_i-\widehat{\phi_i}\|}{N}$	$\frac{\sum[(\theta_i-\widehat{\theta_i})\leq 3°]}{N}$	$\frac{\sum[(\phi_i-\widehat{\phi_i})\leq 3°]}{N}$
		Experiment 1			
T1	SG_M	1.1° (1.9°)	0.4° (2.4°)	1.00 (0.89)	1.00 (0.89)
	SG_S	2.3° (5.6°)	2.0° (6.2°)	0.80 (0.62)	0.85 (0.73)
T2	SG_M	2.2° (3.1°)	5.0° (6.5°)	0.90 (0.78)	0.68 (0.54)
	SG_S	2.9° (6.6°)	5.8° (6.5°)	0.76 (0.60)	0.54 (0.52)
T3	SG_M	1.0° (1.4°)	0.5° (1.9°)	1.00 (0.95)	1.00 (0.82)
	SG_S	1.8° (3.0°)	1.7° (2.8°)	0.90 (0.74)	0.85 (0.73)
		Experiment 2			
T1	SG_M	1.0° (1.8°)	0.7° (1.0°)	1.00 (0.88)	1.00 (0.99)
	SG_S	1.5° (2.2°)	0.9° (2.3°)	0.95 (0.80)	0.98 (0.85)
T2	SG_M	1.0° (2.0°)	2.5° (4.6°)	1.00 (0.86)	0.85 (0.63)
	SG_S	1.8° (3.3°)	3.3° (5.2°)	0.90 (0.75)	0.76 (0.52)
T3	SG_M	0.9° (1.2°)	1.8° (2.8°)	1.00 (0.97)	0.80 (0.74)
	SG_S	2.9° (3.5°)	3.0° (3.0°)	0.80 (0.77)	0.66 (0.65)
		Experiment 3			
T1	SG_M	0.6° (4.2°)	1.4° (8.7°)	1.00 (0.73)	0.85 (0.62)
	SG_S	1.0° (8.8°)	2.8° (9.9°)	0.98 (0.72)	0.68 (0.44)
T2	SG_M	2.1° (5.6°)	4.6° (8.3°)	0.90 (0.65)	0.63 (0.41)
	SG_S	2.8° (8.4°)	4.4° (8.3°)	0.78 (0.54)	0.56 (0.40)
T3	SG_M	1.9° (8.6°)	1.7° (5.4°)	0.95 (0.65)	0.93 (0.71)
	SG_S	2.3° (9.4°)	4.1° (7.1°)	0.78 (0.52)	0.61 (0.48)

derived from observing biological systems.

REFERENCES

[1] D. Browne and L. Kleeman. An advanced sonar ring design with 48 channels of continuous echo processing using matched filters. *2009 IEEE/RSJ International Conference on Intelligent Robots and Systems*, pages 4040–4046, October 2009.

[2] M. K. Obrist, M. B. Fenton, J. L. Eger, and P. A. Schlegel. What ears do for bats - a comparative study of pinna sound pressure transformation in chiroptera. *Jour. of Experimental Biology*, 180:119–152, July 1993.

[3] R. Müller and R. Kuc. Biosonar-inspired technology: goals, challenges and insights. *Bioinspiration and Biomimetics*, 2(4):146–161, December 2007.

[4] J. Tardos, J. Neira, P. Newman, and J. Leonard. Robust mapping and localization in indoor environments using sonar data. *International Journal of Robotics Research*, 21(4):311–330, April 2002.

[5] L. Kleeman. Advanced sonar with velocity compensation. *Int. Journal of Robotics Research*, 23(2):111–126, 2004.

[6] L. Kleeman and R. Kuc. Mobile robot sonar for target localization and classification. *Int. Journal of Robotics Research*, 14(4):295–318, August 1995.

[7] B. Barshan and R. Kuc. A bat-like sonar system for obstacle localization. *IEEE Transactions on Systems, Man and Cybernetics*, 22(4):636–646, July/August 1992.

[8] H. Peremans, K. Audenaert, and J. Van Campenhout. A high-resolution sensor based on tri-aural perception. *IEEE Transactions on Robotics and Automation*, 9(1):36–48, February 1993.

[9] R. Kuc. Three-dimensional tracking using qualitative bionic sonar. *Robotics and Autonomous Systems*, 11(3-4):213–219, December 1993.

[10] H. Akbarally and L. Kleeman. A sonar sensor for accurate 3d target localisation and classification. *Proceedings of 1995 IEEE Int. Conf. on robotics and automation*, 1-3:3003–3008, 1995.

[11] J.A. Jimenez, M. Mazo, J. Urena, A. Hernandez, F. Alvarez, J.J. Garcia, and E. Santiso. Using pca in time-of-flight vectors for reflector recognition and 3-d localization. *IEEE Transactions on Robotics*, 21(5):909–924, October 2005.

[12] J.M. Wotton and J. A. Simmons. Spectral cues and perception of the vertical position of targets by the big brown bat, eptesicus fuscus. *Journal of the Acoustical Society of America*, 107(2):1034–1041, February 2000.

[13] J. Reijniers and H. Peremans. Biomimetic sonar system performing spectrum-based localization. *IEEE Transactions on Robotics*, 23(6):1151–1159, December 2007.

[14] I. Matsuo, J. Tani, and M. Yano. A model of echolocation of multiple targets in 3d space from a single emission. *Journal of the Acoustical Society of America*, 110(1):607–624, July 2001.

[15] R. A. Altes. Angle estimation and binaural processing in animal echolocation. *Journal of the Acoustical Society of America*, 63(1):155–173, 1978.

[16] L.E. Kinsler, A.R. Frey, A.B. Coppens, and J.V. Sanders. *Fundamentals of Acoustics*. Chapman and Hall, London, UK, 4 edition, 2000.

[17] H. Peremans and J. Reijniers. *The CIRCE head: a biomimetic sonar system*, volume LNCS-3696. Springer Verlag, Berlin, DE, 2005.